

ChemComm

Accepted Manuscript



This is an *Accepted Manuscript*, which has been through the Royal Society of Chemistry peer review process and has been accepted for publication.

Accepted Manuscripts are published online shortly after acceptance, before technical editing, formatting and proof reading. Using this free service, authors can make their results available to the community, in citable form, before we publish the edited article. We will replace this *Accepted Manuscript* with the edited and formatted *Advance Article* as soon as it is available.

You can find more information about *Accepted Manuscripts* in the [Information for Authors](#).

Please note that technical editing may introduce minor changes to the text and/or graphics, which may alter content. The journal's standard [Terms & Conditions](#) and the [Ethical guidelines](#) still apply. In no event shall the Royal Society of Chemistry be held responsible for any errors or omissions in this *Accepted Manuscript* or any consequences arising from the use of any information it contains.

COMMUNICATION

One-Step Synthesis and Surface Functionalization of Dumbbell-Like Gold-Iron Oxide Nanoparticles. A Chitosan-Based Nanotheranostic System.

Cite this: DOI: 10.1039/x0xx00000x

Received 00th January 2012,
Accepted 00th January 2012

DOI: 10.1039/x0xx00000x

www.rsc.org/

Nina Kostevsek,^a Erica Locatelli,^b Chiara Garrovo,^c Francesca Arena,^d Ilaria Monaco,^b Ivaylo Petrov Nikolov,^e Saso Sturm,^a Kristina Zuzek Rozman,^a Vito Lorusso,^f Pierangela Giustetto,^f Paola Bardini,^d Stefania Biffi^c and Mauro Comes Franchini^{b*}

Abstract. The first one-step synthesis of dumbbell-like gold-iron oxide nanoparticles has been reported here. Surface functionalization with biocompatible chitosan matrix allowed to obtain a novel targetable diagnostic and therapeutic tool.

Metallic nanoparticles (NPs) with intrinsic theranostic,¹ diagnostic and therapeutic properties can play an important role in biomedical applications and a large number of papers have been focused on these subjects in the last years.² In addition, their surface can be functionalized with biocompatible natural and non-toxic matrix thus giving hybrid organic-inorganic nanotheranostic systems which are capable of delivering their cargos throughout the body.³

Metallic binary systems are considered especially suitable due to their multiple functional features. Among the several possible metals, iron and gold are the most used due to their lack of toxicity and intrinsic properties that are well suited for theranostics.⁴ In addition to the well-known magnetic properties of iron oxide, which account for magnetic-guided delivery towards the target organ, multicomponent systems based on gold and iron are expected to exhibit surface plasmon resonance properties due to the incorporation of gold. This allows for both imaging, such as the novel and non-invasive photoacoustic imaging (PAI),⁵ and for photothermal therapy (PTT).⁶

Gold-iron oxide multicomponent systems have been largely investigated especially in form of core-shell particles.⁷ Even though widely used, the core-shell particles might present the drawbacks since the outer layer is derived from the core, thus limiting the core/shell phase options, the structural quality of the shell, and the ability to control the size of each component. An alternative nanocomposite containing two different metallic NPs are the dumbbell-like (dl) nanoparticles. However, to the best of our knowledge, there are few reports on the synthesis of dumbbell-like gold-iron oxide nanoparticles (dl-Au/Fe₃O₄ NPs). Yu et al.⁸ first described the multistep formation of the dumbbell-like structure through the epitaxial growth of the iron oxide on the Au seeds. Later

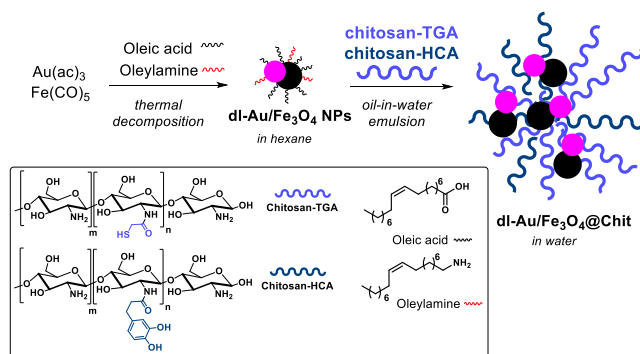
it was shown that such a hybrid structure has a high potential in several applications, such as laser-assisted therapy and magnetic resonance imaging (MRI).⁹ These approaches all exploited a procedure involving several steps, various purifications and long times to obtain the final material, which was then used unmodified and without any functionalization of their surface.

A straightforward synthesis of dl-Au/Fe₃O₄ NPs has never been reported so far, nor has any kind of their surface functionalization, even though this is a key step for their use as hybrid organic-inorganic nanotheranostic systems, a topic which also remains unexplored in nanomedicine.

Herein we describe a simple one-step synthesis for the obtainment of dl-Au/Fe₃O₄ NPs. Moreover, we report a novel method to functionalize the surface of dl-Au/Fe₃O₄ NPs with a natural and highly biocompatible chitosan matrix, thus obtaining a water-stable nanocarrier for theranostics. Finally the potential use of this multicomponent system as PAI contrast agent in phantom and as nano-heater for PTT is demonstrated.

In our one-step synthesis of dl-Au/Fe₃O₄ NPs, both metal precursors were simultaneously added in the same reaction mixture. dl-Au/Fe₃O₄ NPs were prepared by high temperature polyol method with reduction of Au acetate and thermal decomposition of iron pentacarbonyl in the presence of the reducing agent (1,6-hexadecanediol) with oleylamine (OLA) and oleic acid (OA) acting as the capping agents (**Scheme 1**). During the heating, the high difference in the reduction potential between Au and Fe leads to a much faster nucleation of Au NPs. Moreover, due to the presence of oleic acid, Fe forms very stable complex (presumably, iron oleate), which slows the iron nucleation and growth. Therefore, facile reduction of the Au(III) salt enables that Au NPs are first formed in the reaction mixture. Then, at higher temperatures, the presence of the Au NPs catalyzes the decomposition of iron pentacarbonyl and consequently, heterogeneous nucleation of Fe at the surface of the NPs occurs.¹⁰ These nuclei then grow epitaxial and form dl-Au/Fe₃O₄ NPs. TEM images of as-synthesized dl-Au/Fe₃O₄ NPs

taken at lower (80.000x) and higher magnification (300.000x) are shown in **Fig. S1** in the Supporting Information File. Darker Au phase in the dumbbell NP can be easily distinguished from the lighter Fe₃O₄ phase. No agglomerates of the dl-Au/Fe₃O₄ NPs could be found due to the steric stabilization with the surfactants (OLA and OA). The average size of dl-Au/Fe₃O₄ NPs is found to be 7±1 nm.



Scheme 1. Representative scheme for the synthesis of dl-Au/Fe₃O₄@Chit

Fig. 1a shows a representative HAADF-STEM image of interface between individual Au and Fe-oxide NPs at the atomic-resolution. The structural analysis of the corresponding crystal phases confirmed that the bright particle, shown on the left hand-side of the image, corresponds to Au *fcc* structure (inorganic crystal structure database “ICSD” 52700) observed in [101]_{Au} zone axis. On the other hand, the crystal structure of the particle located on the right hand-side of the interface matches perfectly with cubic Fe₃O₄ with the inverse spinel structure (ICSD 65340), which was also observed in [101]_{Fe₃O₄} crystallographic projection. The {111} family of lattice planes measured from the experimental image for Au and Fe₃O₄ was 2.4 Å and 4.8 Å, respectively, which is in good agreement with the literature.⁸ It is worth nothing that there is a 4.4° lattice mismatch between both structures, which is observed in the corresponding FFT, shown as an inset in **Fig. 1a**. The lattice mismatch was determined from (202)_{Au} and (404)_{Fe₃O₄} planes indicated by the red and blue arrows in FFT and in the HAADF-STEM image, respectively. The slightly misaligned crystal lattices are probably the result of the small lattice mismatch (~3%) between theoretical values of Au 2d₁₁₁-(0.471 nm) and Fe₃O₄ d₁₁₁-(0.485 nm) values, which could provoke local structural compensation at the interface enabling the epitaxial growth of the Fe₃O₄ onto the surface of Au.

The capping agents present onto the as-synthesized dl-Au/Fe₃O₄ NPs enabled good steric stabilization in organic solvents. However, for biomedical applications water-based suspensions are required. Modification of dl-Au/Fe₃O₄ NPs surface with specially designed chitosan chains were carried out in order to both replace the native capping agents and to create a highly biocompatible shell able to protect and deliver the dl-Au/Fe₃O₄ NPs within the body. To ensure this aim we exploited, as recently demonstrated by us, the affinity of iron oxide for catechol fragments¹¹ and the one of gold for thiol groups.¹²

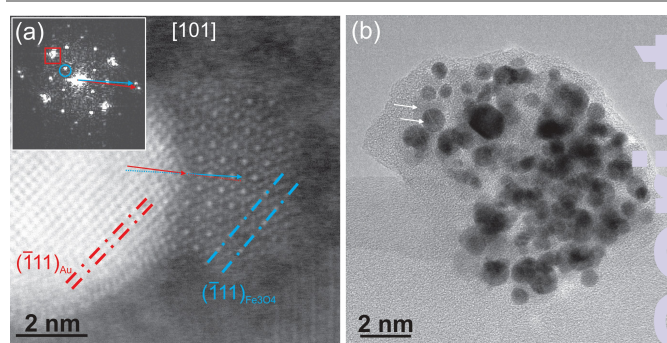


Figure 1: (a) Atomic resolution HAADF-STEM image of interface between Au and Fe₃O₄ particles observed in [101] zone axis with the corresponding diffraction spots for Au and Fe₃O₄ phase indicated in the FFT (inset image) by the rectangle and circle, respectively, (b) TEM image of chitosan encapsulated dl-Au/Fe₃O₄ NPs

Therefore, chitosan biopolymer was modified either with thioglycolic acid (TGA),¹³ thus introducing thiol groups onto its chain (chitosan-TGA), or with hydrocaffeic acid (HCA),¹⁴ thus introducing catechol moieties (chitosan-HCA). Both reagents were linked to the amine groups of chitosan by formation of an amide bond exploiting the 1-Ethyl-3-(3-dimethylaminopropyl)carbodiimide (EDC) coupling reagent.

The anchoring of the two modified chitosan biopolymers onto the NPs surface and consequently the nanocarriers formation were performed by a single, one-pot step, through an oil-in-water emulsion technique (**Scheme 1**). dl-Au/Fe₃O₄ NPs redispersed in chloroform were mixed with the chitosan water-solution and the two phases were then emulsified with a tip probe sonicator, thus ensuring the ligand exchange reaction onto the NPs surface and the formation of a stable nanosystem.

Chitosan-TGA and chitosan-HCA alone, as well as a mixture of the two, were all tested in order to establish the best formation of a stable nanosystem. All the obtained nanosystems were easily purified by magnetic decantation taking advantage of the properties of iron-oxide and redispersed in water before analysis: notably, they are perfectly soluble in water at neutral pH (6.5-7).

A complete characterization by dynamic light scattering (DLS), ζ-potential, atomic absorption spectroscopy (AAS), thermogravimetric analysis (TGA), infrared spectroscopy (IR), UV-Vis and transmission electron microscopy (TEM) was carried out.

dl-Au/Fe₃O₄ NPs embedded in the chitosan-HCA showed a diameter of 140.0 nm but also a high polydispersity index (PDI of 0.560) and poor ζ-potential value of 0.46 mV. On the other hand, it was not possible to synthesize dl-Au/Fe₃O₄ NPs embedded only in chitosan-TGA since any attempt led to aggregation of the particles. The best nanosystem was obtained by the use of both chitosan-HCA and chitosan-TGA together (50/50 w/w): this is characterized by a diameter of 121.2 nm, a low PDI (0.212) and ζ-potential of +37.0 mV (**Fig. S2**). In this case, the higher ζ-potential value, which is due to the protonated amino group of chitosan, and suggested a better coating of dl-Au/Fe₃O₄ NPs surface than Chitosan-HCA alone. Stability of this system in physiological medium and at various pH was also checked: the obtained nanoparticles were incubated in phosphate buffered saline (PBS) at pH 7.4 for two weeks and DLS checked after that. The DLS showed a slightly increased of the mean hydrodynamic diameter, which moved from 120 nm to 130 – 140 nm: this was surely expected due to the long time in the presence of

salts, thus it is possible to consider the particles stable in the tested condition. Moreover the stability of the particles at various pH was checked by recording the change in ζ -potential value and diameter against pH. The graphs (Fig. S3) clearly showed a good stability of the particles between pH 3.5 and 9.5, which is a fairly large interval. In particular, the diameter was never significantly affected, while the Z-potential value, even remaining highly positive, presents a sharp decrease between pH 5.5 and 6.5, due to the pKa of chitosan in this range. Indeed the dl-Au/Fe₃O₄ NPs modified with both Chitosan-TGA and Chitosan-HCA (named from now on as dl-AuFe₃O₄@Chit) showed the best features in terms of size, polydispersivity and stability, resulting from the fact that the iron and gold atoms were exposed on the external, reactive surface of the NPs. In the FT-IR (Fig. S4) the signal of chitosan glycosidic linkage (–C–O–C–) appeared at 1150–1040 nm in the spectrum of dl-Au/Fe₃O₄@Chit, thus confirming the presence of chitosan onto the nanoparticles. In addition, TGA analysis (Fig. S5) showed a typical weight loss (30.3 %) in range temperature between 100–270 °C due to the presence of chitosan on the dl-Au/Fe₃O₄ NPs surface. AAS analysis revealed the incorporation of high payloads into chitosan matrix whereas the concentration was found to be 2.8 mM in iron and 8.0 mM in gold. UV-Vis spectrum showed a λ maximum at 550 nm (Fig. S6). The magnetic properties of the chitosan-coated dl-Au/Fe₃O₄ NPs were measured with a vibrating-sample magnetometer (VSM) at room temperature (298 K) and are presented in Fig. S7. TEM image of the chitosan encapsulated dl-Au/Fe₃O₄ NPs is shown in Fig. 1b and, at lower magnification, in Fig S8. The Au and Fe₃O₄ NPs are shown by the arrows, where Au NP can be observed as objects of a dark contrast, enclosed by relatively brighter the Fe-oxide. The chitosan is manifested by the amorphous structure encapsulating the NPs aggregate. The measured size of the capsules was in the range of 60 to 150 nm, in good agreement with the results obtained by DLS. No free-standing dl-Au/Fe₃O₄ NPs could be found, which indicates successful entrapment of all NPs by the chitosan.

Photo-thermal heating properties of dl-AuFe₃O₄@Chit in aqueous suspension were evaluated in order to provide an initial indication of the PTT performance of the nano-composite. Based on the gold concentration that accounts for the strong optical absorption properties, three different dl-AuFe₃O₄@Chit dilutions (8 mM, 4 mM, 0.4 mM in gold) were tested under three different laser intensities (15 W/cm², 5 W/cm² and 1 W/cm²). The light source used in the experiments is a near-infrared fiber coupled diode laser, the center wavelength of the output radiation is 808 nm and the maximum output power is 25W. Irradiation time was kept constant at 1 minute for each test. Fig. 2a shows the correlation between different NPs dilutions and different irradiation conditions on temperature variations, while Fig. S9 demonstrates representative images taken with the thermocamera before and after laser irradiation with 5W/cm² intensity. The highest concentration of gold (8 mM) irradiated with 15W/cm² causes the highest DeltaT, which almost reaches 60 °C, bringing the solution at 85 °C, near almost to the boiling point. These conditions are obviously not necessary for future PTT, where DeltaT of only 5–10 °C is generally requested.¹⁵ As can be expected, the results shown on Fig. 2a demonstrate that decreasing both the concentration of gold and the laser intensity leads to a decrease of the induced temperature variation.

Photothermal response still remains detectable until a concentration of 0.4 mM in gold, with DeltaT of few degrees.

The photoacoustic imaging analyses were carried out to determine the PA characteristics of the AuFe₃O₄@Chit NPs (Fig. 2b). The *in vitro* tests enabled us to establish the minimum signal intensity threshold exerted by the nanoparticles as detected by the PA system. Even though the λ_{max} of the dl-AuFe₃O₄ NPs is at 550 nm we decided to irradiate at 680 nm since it is more suitable for future *in vivo* biomedical applications. As can be seen in Fig. S10, the signal intensity is suitable for PA analyses, ranging from 8.0 mM to 4.9 mM at 680 nm. Therefore the combination of PTT and PA imaging of AuFe₃O₄@Chit nano-composites was demonstrated at a concentration around 4–5 mM.

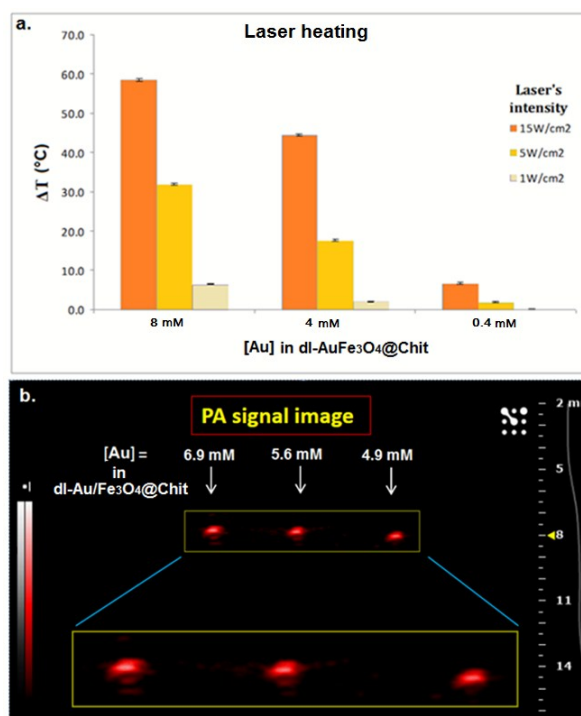


Figure 2. (a) DeltaT induced after irradiation at different laser intensity and concentration. (b) PA intensity signal recorded at 680 nm for dl-AuFe₃O₄@Chit solutions at different concentrations.

In summary, we have developed the first one-step synthesis of dumbbell-like gold-iron oxide nanoparticles and their subsequent entrapment into a biodegradable matrix made of chitosan. The utility of this approach arises from the possibility to manipulate the final dl nanostructures in water and to build targetable nanostructures; these features together with their imaging and therapeutic capabilities herein demonstrated open to future theranostic applications.

Notes and references

^a Department for Nanostructured Materials K-7, Jozef Stefan Institute, Jamova cesta 39 SI-1000, Ljubljana, Slovenia.

^b Department of Industrial Chemistry "Toso Montanari". University of Bologna. Viale Risorgimento 4, 40136 Bologna (Italia). Phone: 051-2093626. Email: mauro.comesfranchini@unibo.it

^c Institute for Maternal and Child Health-IRCCS "Burlo Garofolo", via dell'Istria, 65/1, 34137 Trieste, Italy. Phone: +39-040 3757722.

^d Department of Molecular Biotechnology and Health Sciences. Center of Excellence for Preclinical Imaging (CEIP), University of Torino, Via Ribes 5, 10010, Colletterto Giacosa (TO), Italy

^e Elettra-Sincrotrone Trieste, Strada Statale 14-km 163.5, 34149 Basovizza, Trieste, Italy

^f Ephoran – Multi-Imaging Solutions - Bioindustry Park Silvano Fumero, Colletterto Giacosa, Torino, Italy

† Electronic Supplementary Information (ESI) available: See DOI: 10.1039/c000000x/

- ¹ a) J. Xie, S. Lee, X. Chen, *Adv Drug Deliv Rev.*, 2010, **62**, 1064. b) M. K. Yu, J. Park, S. Jon. *Theranostics*, 2012, **2**(1), 3.
- ² a) A. Naveed, H. Fessi, A. Elaissari. *Drug Discovery Today*, 2012, **17**, 928. b) S. Biffi, R. Voltan, E. Rampazzo, L. Prodi, G. Zauli, P. Secchiero "Applications of nanoparticles in cancer medicine and beyond: optical and multimodal *in vivo* imaging, tissue targeting and drug delivery" *Expert Opin Drug Deliv.* 2015, **9**, 1.
- ³ Y. H. Bae, K. Park. *J. Control. Rel.*, 2011, **153**, 198.
- ⁴ a) D. Ling, T. Hyeon. *Small*, 2013, **9**, 1449. b) K. C. F. Leung, S. Xuan, X. Zhu, D. Wang, C. P. Chak, S. F. Lee, W. K.W. Ho, B. C. T. Chung, *Chem. Soc. Rev.*, 2012, **41**(5), 1911.
- ⁵ J. J. Niederhauser, M. Jaeger, R. Lemor, P. Weber, M. Frenz, *IEEE Trans. Med. Imaging*, 2005, **24**(4), 436.
- ⁶ F. Chen, W. Cai. *Editorial in Nanomedicine*. 2015, **10**, 1.
- ⁷ Z. Ban, Y. A. Barnakov, F. Li, V. O. Golub, C. J. O'Connor. *J. Mat. Chem.*, 2005, **15**(43), 4660.
- ⁸ H. Yu, M. Chen, P. M. Rice, S. X. Wang, R. L. White, S. Sun. *Nano Letters*, 2005, **5**, 379.
- ⁹ a) N. A. Frey, M. H. Phan, H. Srikanth, S. Srinath, C. Wang, S. Sun. *J. Appl. Phys.*, 2009, **105**, 07B502. b) D. K. Kirui, I. Khalidov, Y. Wang, C. A. Batt, *Nanomedicine*, 2013, **9**, 702. c) C. Xu, D. Ho, J. Xie, C. Wang, N. Kohler, E. G. Walsh, J. R. Morgan, Y. E. Chin, S. Sun. *Angew. Chem. Int. Ed. Engl.*, 2008, **47**, 173.
- ¹⁰ E. V. Shevchenko, M. I. Bodnarchuk, M. V. Kovalenko, D. V. Talapin, R. K. Smith, S. Aloni, W. Heiss, A. P. Alivisatos. *Adv. Mater.*, 2008, **20**, 4323.
- ¹¹ E. Locatelli, L. Gil, L. L. Israel, L. Passoni, M. Naddaka, A. Pucci, T. Reese, V. Gomez-Vallejo, P. Milani, M. Matteoli, J. Llop, J. P. Lellouche, M. Comes Franchini, *Int. J. Nanomed.*, 2012, **7**, 6021.
- ¹² a) M. Comes Franchini, J. Ponti, R. Lemor, M. Fournelle, F. Broggi, E. Locatelli. *J. Mater. Chem.*, 2010, **20**, 10908–10914. b) E. Locatelli, W. Bost, M. Fournelle, J. Llop, L. Gil, F. Arena, V. Lorusso, M. Comes Franchini, *J. Nanopart. Res.*, 2014, **16**, 2304-2313. c) D. Gentili, G. Ori, M. Comes Franchini, *Chem. Comm.*, 2009, 5874.
- ¹³ L. Guo, D. D. Yan, D. Yang, Y. Li, X. Wang, O. Zalewski, B. Yan, Wei Lu. *ACS Nano*, 2014, **8**, 5670.
- ¹⁴ K. H. Bae, M. Park, M. J. Do, N. Lee, J. H. Ryu, G. W. Kim, C. G. Kim, T. G. Park, T. Hyeon. *ACS Nano*, 2012, **6**, 5266.
- ¹⁵ A. Bettaieb, P. K. Wrzal, D. A. Averill-Bates. *Hyperthermia: Cancer treatment and beyond*. 2013, Intech.